Thickness dependence of anomalous magnetic behavior in epitaxial $Fe_3O_4(111)$ thin films: Effect of density of antiphase boundaries

J.-B. Moussy, S. Gota, A. Bataille, M.-J. Guittet, and M. Gautier-Soyer
DSM/DRECAM/SPCSI, CEA Saclay, 91191 Gif-sur-Yvette, France

F. Delille and B. Dieny
DSM/DRFMC/SPINTEC CEA Grenoble, 38054 Grenoble Cedex 9, France

F. Ott and T. D. Doan
Laboratoire Léon Brillouin CEA/CNRS, CEA Saclay, 91191 Gif-sur-Yvette, France

P. Warin and P. Bayle-Guillemaud
DSM/DRFMC/SP2M, CEA Grenoble, 38054 Grenoble Cedex 9, France

C. Gatel and E. Snoeck
CEMES-CNRS/Nanomat, 31055 Toulouse cedex 4, France
(Received 15 April 2004; revised manuscript received 23 September 2004; published 22 November 2004)

We study the magnetic behavior of $Fe_3O_4(111)$ thin films with thicknesses between 5 nm and 50 nm. The films are epitaxially grown on α-$Al_2O_3(0001)$ single crystals by atomic-oxygen-assisted molecular beam epitaxy. The $Fe_3O_4(111)$ thin films exhibit high structural order with sharp interfaces and low roughness and exhibit a Verwey transition for thicknesses above 8 nm. However, the samples have magnetic properties that deviate from the bulk ones. The magnetic moment varies between $2.4\mu_B$ for 5-nm-thick film and $3.2\mu_B$ for 50-nm-thick film in a field of 1.2 T, which is lower than that of bulk samples ($4.1\mu_B/Fe_3O_4$ formula). Still the magnetic saturation is never reached, even in fields as large as 2 *T*. The thinner the film, the slower the approach to saturation. Structural analysis, performed using high-resolution transmission electron microscopy, reveals the presence of antiphase boundaries (APB's), the density of which decreases when the thickness increases. Using a model of ferromagnetic domains separated by antiferromagnetically sharp interfaces, we show that the slow approach to saturation observed in the films as a function of thickness is driven by the APB density.

DOI: 10.1103/PhysRevB.70.174448 PACS number(s): 75.70.Ak, 75.60.−d, 81.15.Hi

I. INTRODUCTION

In the last decade effects related to spin-dependent transport like giant magnetoresistance[1–3] (GMR) and tunneling magnetoresistance[4] (TMR) in thin magnetic multilayers have stimulated a considerable interest. These physical properties can be exploited in a variety of advanced devices such as highly sensitive magnetic sensors (e.g., read heads for magnetic recording) and nonvolatile magnetic memories[5,6] (MRAM's). Spin polarization is the driving force of these phenomena, so many research groups focus their attention on the elaboration of thin layers of half-metallic ferromagnets (HMF's)—i.e., materials fully polarized at the Fermi level. The use of HMF electrodes in magnetic tunnel junctions (MTJ's) opens up new performances in spin electronics, leading to potential TMR values much higher than those obtained with usual ferromagnetic electrodes.[7] One of the predicted HMF's is magnetite Fe_3O_4,[8–10] which exhibits a high Curie temperature (T_c=858 K) so that one can expect the HMF character to remain significant at room temperature.[11] Nevertheless, the possible applications of magnetite layers in devices rely on the assumption that the physical properties are the same as those of bulk material. Unfortunately, the physical properties such as resistivity, magnetoresistance,[12,13] or magnetic behavior[14] of Fe_3O_4 thin films strongly deviate from bulk properties. These anomalous behaviors have often been ascribed to the presence of antiphase boundaries[15] (APB's). The APB's are growth defects resulting from the nucleation of islands which correspond to a stacking fault in the iron cation sublattice. It was first believed that the APB's formed at the very first stages of the growth and that the domain size was fixed. However, Eerenstein *et al.*[16] recently showed in a thorough study that the APB's anneal out via a diffusive mechanism, even at moderate growth temperature. The domain size increases with deposition time, and the density of APB's decreases as well when the thickness of the Fe_3O_4 film increases. The magnetotransport properties of $Fe_3O_4(001)$ thin films have been carefully measured as a function of thickness and a clear relationship between the resistivity and the APB domain size has been found.[17]

The magnetic properties of thin films also differ significantly from those of bulk samples: the magnetization at high field is considerably reduced with respect to the bulk value and it is not possible to saturate magnetite thin films.[14] To our knowledge, even though it has been often claimed in the literature that these two results were strongly related to the presence of APB's, no specific investigation of the link between the microstructure (density of APB's) and the mag-

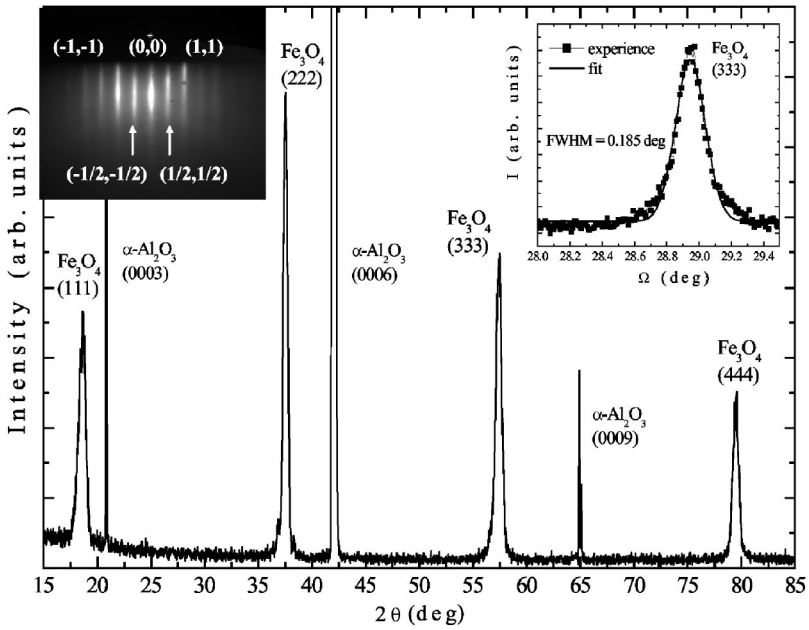

FIG. 1. Typical XRD pattern of a 15-nm-thick Fe_3O_4 (111) film. The rocking curve of the (333) peak is shown in the right inset. Left inset: RHEED pattern of the Fe_3O_4 (111) thin film when the incident electron beam is along the $[1\bar{1}00]$ direction of the alumina substrate in the real space. The probed rods in the reciprocal space are labeled with respect to the base vectors a^* and b^*.

netic properties of magnetite thin films has been reported yet. The purpose of the present work is to investigate the magnetic properties of Fe_3O_4 thin films of increasing thickness, so as to relate quantitatively the density of APB's with the magnetic behavior of the $Fe_3O_4(111)$ epitaxial films, particularly the approach to saturation. We carefully ensured that the only difference between the films is their thickness, all samples being grown exactly in the same way.

The paper is organized as follows. The preparation and *in situ* characterization of $Fe_3O_4(111)$ thin films are briefly summarized in Sec. II. In Sec. III, the perturbed magnetic behavior is evidenced by two complementary techniques: polarized neutron reflectometry (PNR) and vibrating sample magnetometry (VSM). In Sec. IV, the structural analysis of the films by transmission electron microscopy (TEM), especially the APB domain structure, is investigated. Finally the correlations between the APB density with respect to the thickness and the magnetic properties of $Fe_3O_4(111)$ thin films are discussed in Sec. V.

II. MOLECULAR BEAM EPITAXY GROWTH AND CHARACTERIZATION OF $Fe_3O_4(111)$ THIN FILMS

Fe_3O_4 samples of thicknesses ranging from 3 nm to 50 nm were prepared by molecular beam epitaxy (MBE) on α-$Al_2O_3(0001)$ substrates in an ultrahigh-vacuum (UHV) chamber at a residual pressure of 10^{-8} mbar during deposition (base pressure of 10^{-11} mbar). A description of the MBE setup and the growth conditions of the different iron oxide phases [$Fe_3O_4(111)$, α-$Fe_2O_3(0001)$] using a dc oxygen plasma source are detailed in previous papers.[18,19] All the $Fe_3O_4(111)$ films studied in this paper were grown using a new water-cooled radio frequency (rf) plasma source.[20] A constant molecular oxygen pressure (p) was maintained in a cylindrical quartz cavity with the use of a pressure regulator (baratron). Then, a rf power (P) was applied to activate an oxygen plasma. The oxidation efficiency was higher than with the previous dc one because the atomic oxygen density in the plasma was higher. The optimal plasma conditions for the growth of $Fe_3O_4(111)$ were $p=0.1$ torr and $P=350$ W. The oxide deposition rate has been measured by a quartz microbalance and set to 0.2 nm/min. The sample holder, maintained at a temperature of 450 °C, was rotated during growth to avoid inhomogeneous deposition. The growth of each sample was monitored in real time by reflection high-energy electron diffraction (RHEED). The purity and stoichiometry of the films were also checked *in situ* using x-ray photoemission spectroscopy[18,19] (XPS). A selected set of samples, with thicknesses 5 nm, 8 nm, 15 nm, 25 nm, and 50 nm has been studied by PNR and high-resolution transmission electron microscopy (HRTEM) and dark-field TEM.

Figure 1 shows the typical x-ray diffraction (XRD) pattern of a 15-nm-thick $Fe_3O_4(111)$ film using the Cu $K\alpha_1$ radiation. The XRD pattern exhibits only (hhh) peaks corresponding to the (111) orientation of the Fe_3O_4 phase. The coherence length along the (111) growth direction obtained from the full width at half maximum (FWHM) of the (333) peak is 15 nm, which matches with the estimated film thickness. This means that crystallographic order perpendicular to the (111) growth direction is achieved throughout the film. The rocking curve obtained on this (333) peak ($\Delta\Omega = 0.185°$) shows the high texture of the layer. The RHEED pattern of Fe_3O_4 along the $[1\bar{1}00]$ direction of the α-Al_2O_3 substrate (left inset of Fig. 1) is characteristic of magnetite: one sees additional (1/2, 1/2)-type rods typical of the inverse spinel phase and sharp diffraction streaks, implying a flat single crystalline growth.[19]

III. MAGNETIC BEHAVIOR

The magnetic properties of epitaxial $Fe_3O_4(111)$ films have been studied by two complementary techniques: PNR and VSM. PNR consists in measuring the reflection of a

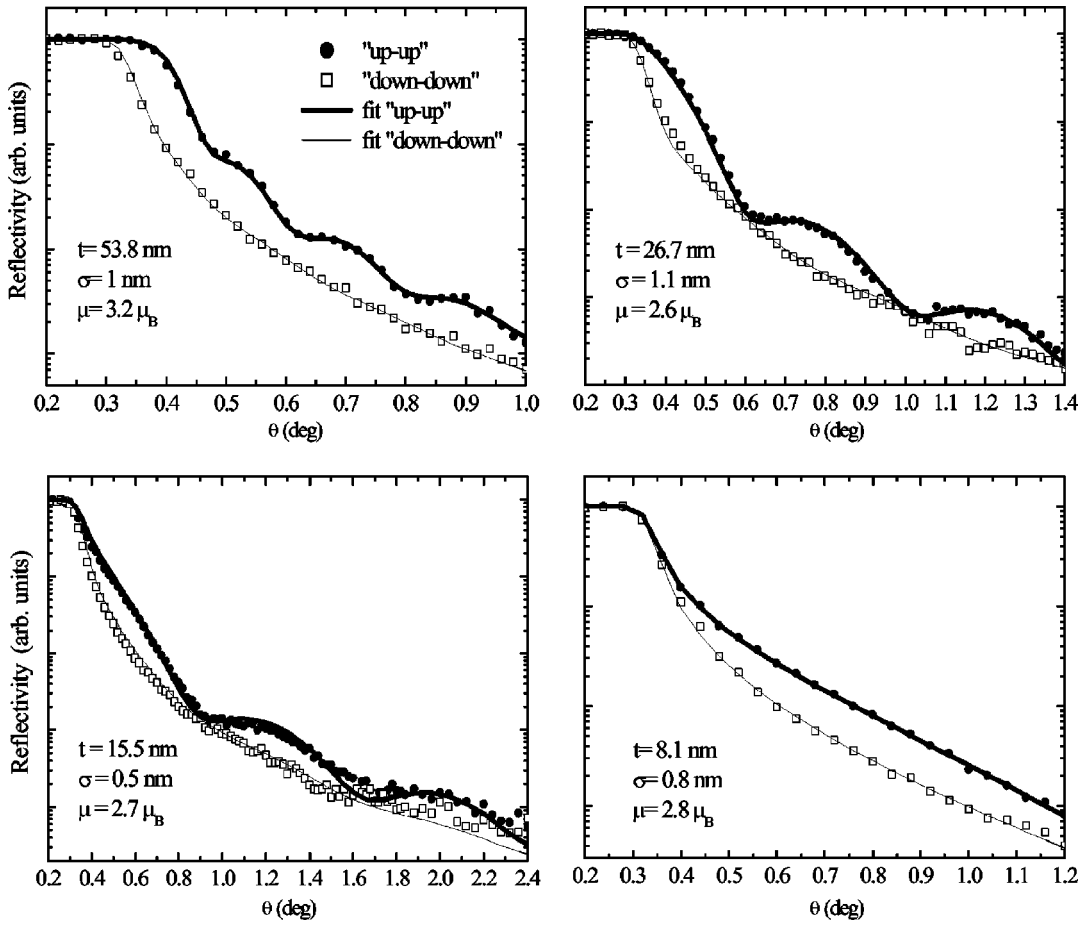

FIG. 2. Polarized neutrons reflectivity measurements of 50-, 25-, 15-, and 8-nm-thick Fe_3O_4 (111) thin films in a 1.2-T in-plane field at $T=300$ K. The circles (squares) represent the up-up (down-down) reflectivity curves. The numerical adjustments are plotted in solid lines.

polarized neutrons beam on a magnetized thin film at grazing incidence[21,22] and is especially suited to the measurement of magnetization and magnetic profile in thin films. This method also retrieves information on the chemical composition as well as on the thickness and the roughness of the films. Figure 2 shows a set of PNR curves for 50-, 25-, 15-, and 8-nm-thick Fe_3O_4 thin films obtained at the Laboratoire Léon Brillouin on the PRISM reflectometer (in-plane applied field of 1.2 T). The dotted curves (respectively, squared) correspond to the reflection of incident up-polarized (respectively, down-polarized) neutrons. Oscillations are clearly observed on the reflectivity up-up curves of the four films, except for the 8-nm film, as expected from the relationship between the oscillation period, the neutron wavelength, and film thickness. The lack of oscillations on the reflectivity down-down curves of the four films is accidental and is related to the interaction potential of the magnetic layer which is close to the potential of the alumina substrate for this spin direction. The numerical fits are represented by solid lines. These reflectivity curves were numerically calculated using conventional optical formulas, allowing the different parameters (nuclear scattering amplitude, density, thickness, surface roughness, and magnetic moment) to vary until a good agreement with the experimental data is obtained. It may happen that additional layers are required in the model at the substrate/film or film/vacuum interfaces to get a satisfactory fit. A single layer with a homogeneous magnetic moment throughout the film reproduced experimental data for each of the measured samples. Thickness (t) and surface roughness (σ) parameters are consistent with other structural characterizations [atomic force microscopy (AFM) and x-ray reflectivity, not shown in this paper]. However, the fit parameter of the magnetic moment (μ) is always lower than the bulk value of $4.1\mu_B$/formula.[23] The values obtained for our films of thicknesses ranging from 5 nm to 50 nm vary respectively, between $2.4\mu_B(\pm 0.2)$/formula or 3×10^5 A/m and $3.2\mu_B(\pm 0.2)$/formula or 4×10^5 A/m—i.e., between 62% and 78% of the bulk value (see Table I). These results are in agreement with previous works.[24,25]

The magnetic hysteresis loops of the 50-, 25-, 15-, and 8-nm-thick $Fe_3O_4(111)$ films have also been measured at room temperature up to 2 T using a VSM. The field was applied along the $[1\bar{1}20]$ axis in plane and along the [0001] axis out of plane of the α-$Al_2O_3(0001)$ substrate (see Fig. 3, where the $[-0.3-0.3]$ T part of the loop is shown). A significant diamagnetic contribution from the substrate had to be accounted for. The susceptibility of each blank α-Al_2O_3 substrate has thus been measured before deposition and carefully subtracted from the magnetization data. All the thin films exhibit an easy in-plane magnetization due to the shape anisotropy. No magnetocrystalline anisotropy within the plane of the films was observed. The remanent magnetization

TABLE I. Magnetic and structural properties of epitaxial $Fe_3O_4(111)$ thin films.

t (nm)	μ (μ_B)	M_r/M_s (1.2 T) (%)	$\mu_0 H_c$ (T)	T_V (K)	Average domain size (nm)
50	3.2	66.8	0.0353	118	50
25	2.6	57.4	0.0384	120	-
15	2.7	50.6	0.0383	105	25
8	2.8	32.6	0.0258	-	10
5	2.4	20.8	0.0143	-	-

reaches 67% of the magnetization at 1.2 T for the thicker film. The observed coercive field $\mu_0 H_c$ is around 0.038 T for thickness above 15 nm which is close to the bulk value of 0.031 T (Ref. 14) (see Table I). We also note the lack of saturation of hysteresis loops and virgin curves even up to 2 T. Not only is the magnetization lower than the bulk value but it also does not seem to reach saturation in the range investigated, while bulk magnetite does.

The insets of each magnetic loop show the temperature dependence of the low-field in-plane susceptibility (χ). Here we focus on the shape of the temperature dependence of χ. The decrease of the susceptibility around $T=100$–120 K for the 50-, 25-, and 15-nm-thick films is characteristic of the Verwey transition.[26,27] This phase transition consists for bulk magnetite in a sharp drop of conductivity by two orders of magnitude together with a magnetic and slight structural transition, and has been the subject of many experimental and theoretical investigations over the last 60 years. The transition temperature is 120 K in the bulk, but a decrease of the Verwey temperature (T_v) has been reported for thin films.[14,28,29] Different explanations have been put forward, such as the presence of cation vacancies, oxygen

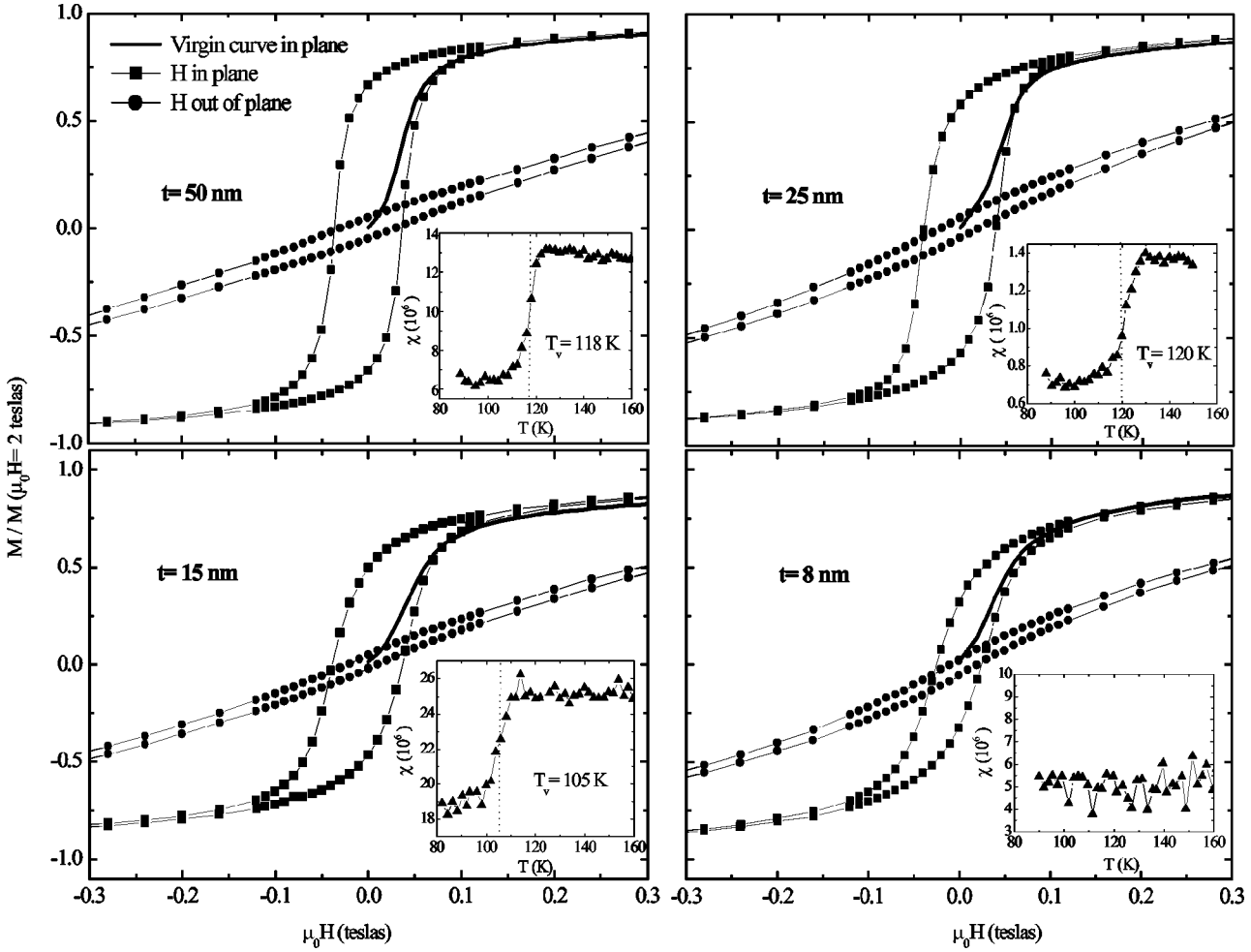

FIG. 3. Magnetic hysteresis loops and virgin curves by VSM measurement of 50-, 25-, 15-, and 8-nm-thick Fe_3O_4 (111) thin films at $T=300$ K after subtraction of the substrate diamagnetic contribution. Inset: temperature dependence of the susceptibility at low field. The decrease of the susceptibility related to the presence of the Verwey transition can be observed for thickness above 8 nm.

nonstoichiometry,[30,31] residual strain resulting from the lattice mismatch with the substrate,[29,32] or difference in thermal expansion coefficients between substrate and the Fe_3O_4 thin film.[33] The presence of the Verwey transition around 120 K in our 50- and 25-nm-thick films proves the high crystalline quality and good stoichiometry of thin films. However, the Verwey temperature is lower for the 15-nm-thick film (T_v = 105 K) and no transition is observed for the 8-nm-thick film, at least above 90 K. Wright *et al.* evidenced very recently that long-range order of the Fe^{2+} and Fe^{3+} ions at the octahedral sites was necessary for the Verwey transition to occur.[34] Indeed, these octahedral coordinated sites are those involved in the conduction process—i.e., thermally activated hopping of electrons between Fe^{2+} and Fe^{3+}. Eerenstein *et al.* reported no Verwey transition within their transport measurements when the thickness of the film was below 25 nm.[17] It was suggested that in very thin films, where the APB density is expected to be very high, the domain size could be so small that the long-range order necessary required for the Verwey transition would be inhibited. As the structural characterizations of the films of the present study did not evidence significant differences between the thickest films (50 nm, 25 nm) and the thinnest (15 nm, 8 nm), except a difference in the APB density (see Sec. IV) the lower transition temperature of the 15-nm film and the lack of transition in the 8-nm one are likely related to this decrease of the long-range order.

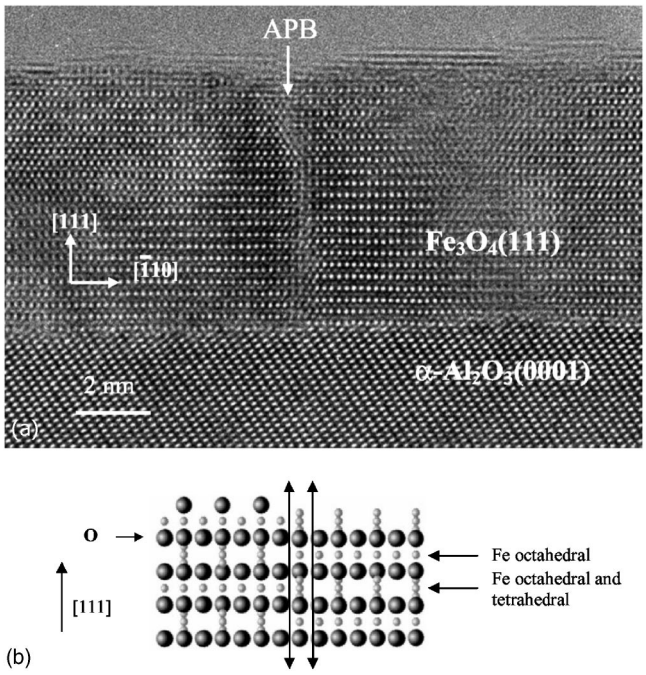

FIG. 4. (a) Cross-sectional HRTEM image of a 15-nm-thick Fe_3O_4 (111) thin film along the $[11\bar{2}]$ direction with the presence of an APB. (b) Sketch of the stacking of (111) atomic layers: the oxygen lattice is undisturbed across the APB while the iron lattice is shifted by a ⟨220⟩ translation vector.

IV. TEM STUDY OF ANTIPHASE BOUNDARIES

In order to study the relationship between anomalous magnetic behavior and microstructure, both cross-section and plane-view TEM analyses were performed in samples with different thicknesses of 50 nm, 15 nm, and 8 nm. HRTEM studies of Fe_3O_4(001) thin films grown on MgO(001) by sputtering[14,35] or by MBE[36–38] have been reported in the literature. A HRTEM study of Fe_3O_4(111) films grown on Pt(111) by iron deposition and subsequent oxidation has been also recently published.[39] Nevertheless, to our knowledge, no HRTEM investigations have been reported yet on Fe_3O_4(111) grown on α-Al_2O_3(0001).

Figure 4 shows a representative cross-sectional HRTEM image of the 15-nm-thick film studied along the $[11\bar{2}]$ direction. It evidences the abruptness of the interface and the high quality of the epitaxy between the Fe_3O_4(111) and α-Al_2O_3(0001) substrates. No other iron oxide phases were detected at the interface. HRTEM image simulations (not shown) were carried out with the EMS software[40] using the multislice method. The successive planes of the stacking sequence in the [111] direction are —O—Fe_{oct}—O—Fe_{tet}—Fe_{oct}—Fe_{tet}—O—. The image simulation allowed us to distinguish in the micrograph bright spots and less intense spots. This variation in the contrast can be attributed to the projection of the Fe tetrahedral and octahedral atoms (located in the three close Fe planes) and Fe octahedral atoms (the single Fe plane). The crystallographic defect observed in the center of the HRTEM cross-section micrograph then corresponds to a shift in the Fe planes stacking as is sketched in Fig. 4(b). It can be unambiguously identified as an APB,[15] which is a stacking defect in the cation sublattice: the oxygen lattice remains undisturbed across the APB while the cation lattice is shifted by a ⟨220⟩ translation vector.

Dark-field TEM plane-view images of the 8-, 15-, and 50 nm-thick films have been realized selecting the 220-type reflections of the Fe_3O_4 structure studied along the ⟨111⟩ zone axis of the magnetite. Figure 5(a) shows the diffraction pattern obtained when studying the α-Al_2O_3(0001)/Fe_3O_4(111) system along such a zone axis. The 220-type reflections of the magnetite and the $11\bar{2}0$ ones of α-Al_2O_3 substrate are reported. The weak reflections located around the main reflections are due to a double diffraction phenomema between the magnetite and α-Al_2O_3 and indicate the perfect epitaxy of the growth over at least a few micron square. In Figures 5(b)–5(d) are reported dark-field images recorded using the Fe_3O_4 220 reflection (arrowed in the diffraction pattern) for samples of different thicknesses. The dark lines correspond to the APB's where a shift of the 220 planes occurs. Similar images were acquired with the 022 and 202 reflections (not shown). Since the only visible APB's are the ones whose translation vector is perpendicular to the reflection used to realize the dark-field TEM image, the real APB density is higher than what is observed in a single 220 dark-field image. However, the proportion of hidden APB's being the same in all the plane-view image, the evolution of the APB density with the thickness of the film studied in a single 220 dark-field image reflects its total evolution.[16] In the 8-nm-thick film [Fig. 5(b)], we observe an

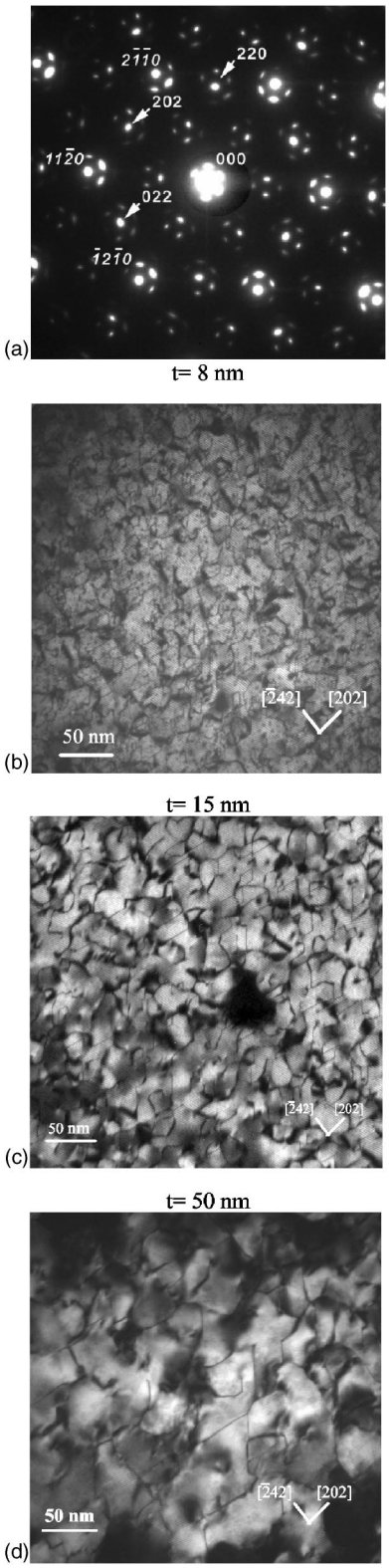

FIG. 5. (a) Diffraction pattern along the ⟨111⟩ zone axis of a magnetite layer. The 220-type reflections of the magnetite and the $11\bar{2}0$ ones of α-Al_2O_3 substrate are reported. (b)–(d) Dark-field TEM images of 8-, 15-, and 50-nm-thick Fe_3O_4 (111) thin films taken with the 220-type reflection along the ⟨111⟩ zone axis. The dark lines correspond to the antiphase boundaries (APB's).

average domain size between APB's of about 10 nm. In the 15-nm-thick film [Fig. 5(c)], the APB density decreases and the mean domain size is close to 25 nm. In the 50-nm-thick film [Fig. 5(d)], this mean domain size increases further to a value close to 50 nm. The domain size then significantly increases with increasing film thickness, and this increase is consistent with the square root law observed in the recent work of Eerenstein *et al.*[16] It should be noticed that this domain size increase is linked to the motion of APB's which is driven by a diffusive mechanism thermally activated. Our results disagree to an earlier report[41] that states that the APB's appear in magnetite films at the very first stages of the growth and that the domain size remains unchanged when increasing the film thickness.

V. DISCUSSION

An anomalous physical behavior in magnetite thin films has been observed regardless of the growth techniques, deposition conditions, or type of substrate.[14] In their pioneering paper, Margulies *et al.* reported a slow approach to saturation compared to the single crystal with only a slight thickness dependence. The origin of this anomalous behavior was ascribed to the presence of APB's, evidenced by TEM.[15,36] Across an APB, a strong antiferromagnetic coupling might exist which modifies the magnetic properties.[15] Thin films can then be described as ferromagnetic domains bounded by APB's with an antiparallel magnetic ordering at the atomically sharp interfaces. In order to quantify the impact of these APB's on the magnetic behavior, Margulies *et al.* and Hibma *et al.* used the model introduced by Dieny *et al.* to explain the magnetization processes in artificial rare earth ferrimagnets.[42] This model describes the approach to saturation of two semi-infinite media separated by Bloch walls neglecting the anisotropy energy and considering only the competition between Zeeman energy, which favors magnetization alignment along the applied magnetic field, and the exchange energy. The minimization of the energy leads to

$$M = M_s(1 - b/H^n), \tag{1}$$

where M is the magnetization, M_s the saturation, b a parameter related to the density of APB's, and n an exponent equal to 0.5 in this model. Several attempts have been made in the literature to correlate the b parameter of the model with the density of APB's; however, no systematic study has been done yet on a set of samples grown in the same way, so that the only variable parameter would be the APB density.

Figure 6 displays the magnetization virgin curves of a bulk sample, along with 50-, 25-, 15-, 8-, and 5-nm-thick films, for a magnetic field up to 1.7 T. The bulk sample quickly reaches saturation, and the virgin curve is fitted by the relation predicted for ferromagnetic crystals by Neel.[43] Virgin curves of thin films can be fitted up to 1.7 T by Eq. (1) (M_s, b, and n are the fit parameters) with an exponent equal to 0.5. For a given applied field, the magnetization M is always lower in the films than in the bulk sample. Moreover, it decreases when the film thickness decreases, hence when the APB density increases. The APB density is simply taken as the fraction of crystallographic defect planes,

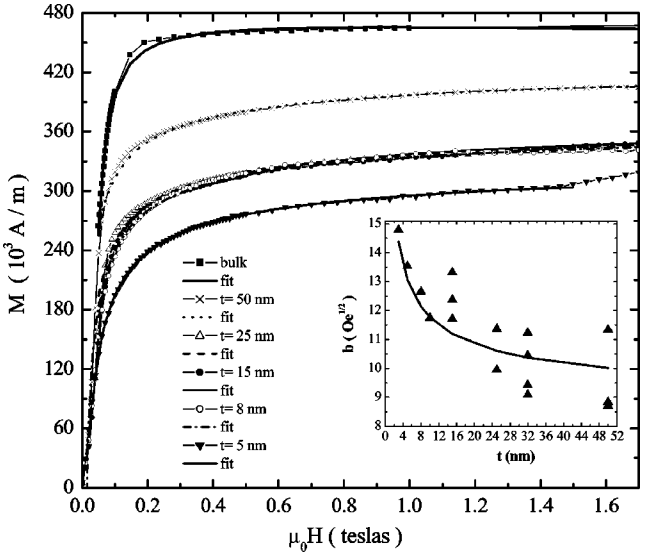

FIG. 6. Virgin magnetization curves at $T=300$ K for a Fe_3O_4 bulk crystal and 50-, 25-, 15-, 8-, and 5-nm-thick Fe_3O_4 (111) thin films with fits to describe the approach to saturation. Inset: b parameter evolution with film thickness.

(sketch at the bottom of Fig. 4), and one assumes the antiferromagnetic coupling only exists between the two planes separated by the APB. Yet the magnetic influence might be much larger, the interaction length being field dependent. While the application of the magnetic field aligns the spins far from the APB, the antiferromagnetic coupling across the APB leads to a progressive rotation of spins at the boundary. Therefore, for a given applied field H, the magnetization projection along H: M_H reaches a minimum value at each APB. Considering the $M_H(x)$ curve, where x is the spatial coordinate perpendicular to the APB, an effective APB thickness can be defined as the FWHM of the peak in $M_H(x)$ centered at the crystallographic APB ($x=0$).[44] Monte Carlo simulations show that this effective APB width decreases when the applied field increases and becomes equal to the crystallographic width (i.e., two crystallographic planes) when the applied field is infinite. However, for finite applied fields, the width of the APB might not be negligible compared to the distance between two crystallographic APB's. The measured magnetization is therefore necessarily lower than the bulk one, due to this decrease of the magnetization at the APB. The magnetic interactions at the APB's can thus explain that the saturation is more difficult to achieve in thin films compared to a single crystal clear of any APB's.

We now focus on the M_s value. Extrapolating Eq. (1) to infinite magnetic field, the b value of 8.4 $(Oe)^{1/2}$ for the 50-nm-thick film and the magnetization obtained at 1.2 T by PNR leads to a M_s of $3.45\mu_B$ significantly lower than the bulk value of $4.1\mu_B$. Different hypotheses can be put forward in order to explain this deficit in M_s. Several papers report the reduction of the magnetization by the presence of a magnetically inactive interface layer.[45] At the first stages of the growth of our thin films, an expanded FeO-like phase has been observed by real time RHEED diffraction.[19] However, the HRTEM micrographs do not show such a phase. Consequently, it probably corresponds to a metastable phase, which transforms into Fe_3O_4 when the Fe and O layers are subsequently grown. The HRTEM micrographs prove that once the growth of the layer is completed, the Fe sublattice is perfectly ordered, giving rise to the $Fe_3O_4(111)$ structure, which is much more thermodynamically stable. Moreover, the PNR measurements showed a homogeneous magnetic moment through the thickness. In addition, this dead layer hypothesis has been also ruled out by conversion-electron Mössbauer spectroscopy[41,46] where it has been shown that the magnetic behavior at the interface is very similar to that of the "bulk" of the sample. Another hypothesis for this magnetization reduction might be the presence of parasitic phases like the antiferromagnetic α-Fe_2O_3 or FeO phase or the ferrimagnetic γ-Fe_2O_3 oxide. No such phases have been evidenced within the accuracy of the characterization methods used in this work like XPS, standard x-ray diffraction, and HRTEM. The Fe $2p$ XPS spectra with the presence of satellite peaks corresponding to Fe^{3+} (Fe_2O_3) or Fe^{2+} (FeO) actually allow one to get information about the iron oxidation state.[18] However, the presence of both Fe^{3+} and Fe^{2+} in magnetite and thus both satellites in the spectra gives rise to an unresolved structure between the two spin-orbit components which is difficult to analyze quantitatively. It is also hard to distinguish the γ-Fe_2O_3 and Fe_3O_4 phases by standard x-ray diffraction since the differences between their lattices parameters are within the error bars of the measurements. Nevertheless, the amount of parasitic phases, if they exist, is in a minor quantity for we observe the Verwey transition for film thicknesses above 15 nm (insets of Fig. 3) which is usually thought to be very sensitive to valence and impurities. So magnetic saturation moment should be likely rather intrinsic to the APB's, although it is not understood in which way the APB density influences the M_s value extrapolated at infinite field. Measurements at very high fields should help to answer this puzzling question.

We finally discuss the approach to saturation. The inset of Fig. 6 shows the b values obtained from the fits. This parameter varies between 8 $(Oe)^{1/2}$ and 15 $(Oe)^{1/2}$ for thicknesses between 50 nm and 3 nm. The values obtained for the 50-nm-thick films are in agreement with the value of 8.8 $(Oe)^{1/2}$ determined by Strijkers et al. (domain size of 50 nm for a 40-nm-thick film).[46] The variation of the b parameter with the film thickness in the inset of Fig. 6 clearly shows that, within the accuracy in the fitting procedure, the b parameter decreases significantly when the film thickness increases—i.e., when the APB domain size increases (as evidenced by TEM in Sec. IV).

Here we have assumed that all APB's were associated with magnetic domain walls. The situation is obviously more complicated, as shown by Eerenstein for different magnetic exchange interactions are competing across the boundaries.[47] Antiferromagnetic coupling is not the only one possible across the boundary, and APB's do not all act as magnetic domain walls. This was also demonstrated by a comparison between atomic and magnetic force microscopy (AFM and MFM) images showing a larger magnetic domain size than the antiphase one.[35] Anyway the present work shows unambiguously that the slow approach to saturation is driven by the APB density.

VI. CONCLUSION

We have grown $Fe_3O_4(111)$ epitaxial films on $Al_2O_3(0001)$ substrates by oxygen-assisted molecular beam epitaxy, with thicknesses ranging from 3 nm to 50 nm, in the very same growth conditions. The magnetic behavior of the films has been investigated using both polarized neutron reflectometry and vibrating sample magnetometry. PNR fits were consistent with a homogenous magnetic layer which magnetic moment at 1.2 T vary between $2.4\mu_B$ and $3.2\mu_B/Fe_3O_4$ formula depending on film thickness. Moreover, the magnetic measurements in fields as large as 1.7 T showed that our films presented a difficulty to reach saturation, as reported in the literature for other magnetite thin films. Dark-field TEM images showed an increase of the crystallographic antiphase domain size when the thickness increases, this increase being consistent with the square root law observed by Eerenstein *et al.* in $Fe_3O_4(001)$ thin films grown on MgO(100). The slow approach to saturation of the virgin curves obtained by VSM was described using a model of a linear chain with ferromagnetic domains antiferromagnetically coupled which lead to an estimate of saturation M_s lower than that of the single crystal, even for the 50-nm-thick film (84% of the bulk value). In view of the high quality of the films, for the Verwey transition observed at the temperature of the bulk for the 50-nm-thick film, this smaller M_s value is also likely linked with the APB density; also, it is not clear yet how the APB density affects this M_s value. High-field experiments should help to understand this. The slow approach to saturation is described by a parameter b (the larger b, the slower the approach to saturation) which is found to increase significantly when the thickness decreases, hence when the APB density increases. This shows unambiguously that the slow approach to saturation is driven by the APB density in the films.

[1] M. N. Baibich, J. M. Broto, A. Fert, F. Nguyen Van Dau, F. Petroff, P. Etienne, G. Creuzet, A. Friederich, and J. Chazelas, Phys. Rev. Lett. **61**, 2472 (1988).

[2] G. Binasch, P. Grünberg, F. Saurenbach, and W. Zinn, Phys. Rev. B **39**, 4828 (1989).

[3] B. Dieny, V. S. Speriosu, S. S. P. Parkin, B. A. Gurney, D. R. Wilhoit, and D. Mauri, Phys. Rev. B **43**, 1297 (1991).

[4] J. S. Moodera, L. R. Kinder, T. M. Wong, and R. Meservey, Phys. Rev. Lett. **74**, 3273 (1995).

[5] See, for example, the web site of IBM Almaden Research Center: http://www.almaden.ibm.com/sst/

[6] J. M. Daughton, Thin Solid Films **216**, 162 (1992); J. Appl. Phys. **81**, 3758 (1997).

[7] M. Viret, M. Drouet, J. Nassar, J.-P. Contour, C. Fermon, and A. Fert, Europhys. Lett. **39**, 545 (1997).

[8] A. Yanase and K. Siratori, J. Phys. Soc. Jpn. **53**, 312 (1984).

[9] Z. Zhang and S. Satpathy, Phys. Rev. B **44**, 13 319 (1991).

[10] Y. S. Dedkov, U. Rüdiger, and G. Güntherodt, Phys. Rev. B **65**, 064417 (2002).

[11] P. Seneor, A. Fert, J.-L. Maurice, F. Montaigne, F. Petroff, and A. Vaures, Appl. Phys. Lett. **74**, 4017 (1999).

[12] J. M. D. Coey, A. E. Berkowitz, Ll. Balcells, F. F. Putris, and F. T. Parker, Appl. Phys. Lett. **72**, 734 (1998).

[13] M. Ziese and H. J. Blythe, J. Phys.: Condens. Matter **12**, 13 (2000).

[14] D. T. Margulies, F. T. Parker, F. E. Spada, R. S. Goldman, J. Li, R. Sinclair, and A. E. Berkowitz, Phys. Rev. B **53**, 9175 (1996).

[15] D. T. Margulies, F. T. Parker, M. L. Rudee, F. E. Spada, J. N. Chapman, P. R. Aitchison, and A. E. Berkowitz, Phys. Rev. Lett. **79**, 5162 (1997).

[16] W. Eerenstein, T. T. M. Palstra, T. Hibma, and S. Celotto, Phys. Rev. B **68**, 014428 (2003).

[17] W. Eerenstein, T. T. M. Palstra, T. Hibma, and S. Celotto, Phys. Rev. B **66**, 201101(R) (2002).

[18] S. Gota, E. Guiot, M. Henriot, and M. Gautier-Soyer, Phys. Rev. B **60**, 14 387 (1999); Surf. Sci. **454–456**, 796 (2000).

[19] S. Gota, J.-B. Moussy, M. Henriot, M.-J. Guittet, and M. Gautier-Soyer, Surf. Sci. **482–485**, 809 (2001).

[20] The new rf plasma source was manufactured by the ADDON company: http://www.addon-mbe.com/

[21] G. P. Felcher, R. Felici, R. T. Kampwirth, and K. E. Gray, J. Appl. Phys. **57**, 3781 (1985).

[22] F. Ott, M. Viret, R. Borges, R. Lyonnet, E. Jacquet, C. Fermon, and J.-P. Contour, J. Magn. Magn. Mater. **211**, 200 (2000).

[23] B. D. Cullity, *Introduction to Magnetic Materials* (Addison-Wesley, Reading, MA, 1972).

[24] T. Furubayashi, J. Appl. Phys. **93**, 8026 (2003).

[25] A. R. Ball, H. Fredrikze, D. M. Lind, R. M. Wolf, P. J. H. Bloemen, M. T. Rekveldt, and P. J. van der Zaag, Physica B **221**, 388 (1996).

[26] E. W. J. Verwey, Nature (London) **144**, 327 (1939).

[27] L. R. Bickford, Phys. Rev. **76**, 137 (1949).

[28] G. Q. Gong, A. Gupta, G. Xiao, W. Qian, and V. P. Dravid, Phys. Rev. B **56**, 5096 (1997).

[29] X. W. Li, A. Gupta, G. Xiao, and G. Q. Gong, J. Appl. Phys. **83**, 7049 (1998).

[30] V. A. M. Brabers, F. Walz, and H. Kronmüller, Phys. Rev. B **58** 14 163 (1998).

[31] R. Aragon, D. J. Buttrey, J. P. Shepherd, and J. M. Honig, Phys. Rev. B **31**, 430 (1985).

[32] G. K. Rozenberg, G. R. Hearne, M. P. Pasternak, P. A. Metcalf, and J. M. Honig, Phys. Rev. B **53**, 6482 (1996).

[33] P. J. van der Zaag, W. F. J. Fontijn, P. Gaspard, and R. M. Wolf, J. Appl. Phys. **79**, 5936 (1996).

[34] J. P. Wright, J. P. Attfield, and P. G. Radaelli, Phys. Rev. Lett. **87**, 266401 (2001).

[35] J.-F. Bobo, D. Basso, E. Snoeck, C. Gatel, D. Hrabovsky, J.-L. Gauffier, L. Ressier, R. Mamy, S. Visnovsky, J. Hamrle, J. Teillet, and A. Fert, Eur. Phys. J. B **24**, 43 (2001).

[36] T. Hibma, F. C. Voogt, L. Niesen, P. A. A. van der Heijden, W. J. M. de Jonge, J. J. T. M. Donkers, and P. J. van der Zaag, J. Appl. Phys. **85**, 5291 (1999).

[37] S. Celotto, W. Eerenstein, and T. Hibma, Eur. Phys. J. B **397**, 43 (2003).

[38] R. M. Wolf, A. E. M. de Veirman, P. van der Sluis, P. J. van der Zaag, and J. B. F. aan de Stegge, in *Epitexial Oxide Thin Films and Heterostantures*, edited by D. K. Fork, J. M. Phillips, R. Ramesh, and R. M. Wolf, MRS Symisic Proceedings No. 341 (Materials Research Society, Pittsburgh, 1994), p. 23.

[39] V. V. Roddatis, D. S. Su, C. Kuhrs, W. Ranke, and R. Schlögl, Thin Solid Films **396**, 78 (2001).

[40] P. A. Stadelmann, EMS-A software package for electron diffraction analysis and HREM image simulation in material science: Ultramicroscopy **21**, 131 (1987); P. A. Stadelmann (unpublished).

[41] F. C. Voogt *et al.*, Phys. Rev. B **57**, R8107 (1998).

[42] B. Dieny, D. Givord, and J. M. B. Ndjaka, J. Magn. Magn. Mater. **93**, 503 (1991).

[43] L. Néel, J. Phys. Radium **9**, 184 (1948).

[44] L. Berger, Y. Labaye, O. Crisan, J.-M. Greneche, and J.-M. D. Coey, J. Appl. Phys. **91**, 7634 (2002).

[45] P. A. A. van der Heijden, P. J. H. Bloemen, J. M. Gaines, J. T. W. M. van Eemeren, R. M. Wolf, P. J. van der Zaag, and W. J. M. de Jonge, J. Magn. Magn. Mater. **159**, L293 (1996).

[46] G. J. Strijkers, J. T. Kohlhepp, P. A. A. van der Heijden, H. J. M. Swagten, W. J. M. de Jonge, and J. M. Gaines, J. Appl. Phys. **85**, 5294 (1999).

[47] W. Eerenstein, Ph.D. thesis, University of Groningen, 2003.